ACID PROPERTIES AND MORPHOLOGY OF SAPO-11 MOLECULAR SIEVE CONTROLED BY SILICA SOURCE

Marat Agliullin, Yury Kolyagin, Dmitriy Serebrennikov, Nellya Grigor'Eva, Andrey Dmitrenok, Valery Maistrenko, Eddy Dib, Svetlana Mintova, Boris Kutepov

▶ **To cite this version:**

Marat Agliullin, Yury Kolyagin, Dmitriy Serebrennikov, Nellya Grigor'Eva, Andrey Dmitrenok, et al.. ACID PROPERTIES AND MORPHOLOGY OF SAPO-11 MOLECULAR SIEVE CONTROLED BY SILICA SOURCE. Microporous and Mesoporous Materials, 2022, 338, pp.111962. 10.1016/j.micromeso.2022.111962 . hal-04295884

HAL Id: hal-04295884
https://hal.science/hal-04295884

Submitted on 20 Nov 2023

HAL is a multi-disciplinary open access archive for the deposit and dissemination of scientific research documents, whether they are published or not. The documents may come from teaching and research institutions in France or abroad, or from public or private research centers.

L'archive ouverte pluridisciplinaire **HAL**, est destinée au dépôt et à la diffusion de documents scientifiques de niveau recherche, publiés ou non, émanant des établissements d'enseignement et de recherche français ou étrangers, des laboratoires publics ou privés.

ACID PROPERTIES AND MORPHOLOGY OF SAPO-11 MOLECULAR SIEVE CONTROLED BY SILICA SOURCE

Agliullin M.R.[1], Kolyagin Yu G. [3], Serebrennikov D.V.[1], Grigorieva N.G.[1], Dmitrenek A.C. [4], Maistrenko V.N.[5], Dib E.,[2] Mintova S.[2], Kutepov B.I.[1]

[1]*Institute of Petrochemistry and Catalysis, UFRC RAS (IPC RAS), Russia, Ufa st. Prospekt Oktyabrya 141, 450075*

[2]*Laboratoire Catalyse et Spectrochimie, Normandie University, ENSICAEN, UNICAEN, CNRS, France, Caen, 6 Bd Marechal Juin, 14050*

[3]*Department of Chemistry, Moscow State University, Russia, Moscow, Lenin Hills 1/3, 119991*

[4]*N.D. Zelinsky Institute of Organic Chemistry RAS, Russia, Moscow, Leninsky prospect, 47, 119991*

[5]*Bashkir State University, Russia, Ufa, st. Zaki Validi, 32, 450076*

ABSTRACT: This paper reports on the control of strong acid sites in SAPO-11 molecular sieve crystals using different silica sources. The crystallization process of the SAPO-11 molecular sieves was performed using silicon sources with different particle sizes, i.e., fumed silica (200 nm), colloidal silica (22 nm), and SiO_2 sol prepared by the sol-gel method (4 nm). The SiO_2 sol proved to have a significant effect on the acidic properties, morphology and crystal size of SAPO-11 molecular sieve. Moreover, more efficient incorporation of silicon is achieved, providing an increased concentration of acid sites. The SAPO-11 intergrown crystals with a size of 100 -300 nm exhibited hierarchical pore structure (S_{BET} – 250 m^2/g and V_{meso} – 0.27 cm^3/g) were synthesized using the SiO_2 sol precursor. The SAPO-11 molecular sieves were tested in the reaction of a-methylstyrene dimers synthesis. The SAPO-11 samples, synthesized by SiO_2 sol showed the highest monomer conversion and linear dimer selectivity.

KEYWORDS: *zeolites, SAPO-11 silicoaluminophosphate, SAPO-11 nanosized crystals, sol-gel method, dimerization of a-methylstyrene*

1. Introduction

The synthesis of silicoaluminophosphate SAPO-n molecular sieves was first reported by Wilson et al. in 1984 [1]. Currently, they are the second most important class of zeo-type materials. New catalytic processes using the SAPO-34 silicoaluminophosphates have been developed over the past 20 years. Honeywell UOP and Dalian Institute of Chemical Physics have worked out on SAPO-34 based processes for production of lower olefins from methanol using

the methanol-to olefin (MTO) [2] while the SAPO-11 based catalyst was used for isodewaxing of oils and diesel fuels as proposed by Chevron [3,4]. The widespread interest in SAPO-n is caused by a wide variety of structures differing in both the pore size (examples: SAPO-18: 3.8*3.8Å, SAPO-5: 7.3*7.3Å, SAPO-8: 12.7*12.7Å, etc.), and dimensionality of the channels (1D - SAPO-11, 2D - SAPO-40, 3D - SAPO-50) [5]. Furthermore, they are characterized by the presence of moderately strong Brønsted acid sites (BAS)and hydrothermal stability.

Brønsted acid sites in SAPO-n are formed as a result of isomorphic incorporation of silicon atoms into the aluminophosphate framework structures. The incorporation of silicon in SAPO-n molecular sieves was suggested to proceed by two different mechanisms, i.e. the SM2 and SM2+SM3 [6-8]. According to the SM2 type, silicon atoms isomorphically substitute for phosphorus atoms, and the so-called *single* incorporation occurs to form moderately strong Brønsted acid sites uniformly distributed within the crystals volume. While the SM2+SM3 mechanism implies incorporation of silicon atoms in the form of silicate islands of various sizes within the crystals. In this case, stronger Brønsted acid sites are formed, localized mainly on the surface of the crystals. Thus, by controlling the process of incorporation of silicon atoms one can control the strength and concentration of acid sites, as well as their localization in SAPO-n molecular sieves.

Among the wide variety of SAPO-n molecular sieves, the SAPO-11 molecular sieve with AEL type framework topology is of particular interest due to the one-dimensional channel system with elliptical pores of size of 4.0×6.5Å, which is comparable in size to many industrially important organic molecules. Bifunctional catalysts based on SAPO-11 molecular sieve offer high selectivity for hydroisomerization of C_{7+} higher n-paraffins [9-11]. Furthermore, SAPO-11 molecular sieve is a promising catalyst for isomerization of n-butene to isobutene [12], cyclohexanone oxime to caprolactam [13,14], and for methylation of aromatic hydrocarbons [15,16].

The main research focus is on the synthesis of SAPO-11 with various particle sizes and hierarchical pore structures toward reduction of diffusion limitations [17]. This synthesis procedures were designed to control the process of incorporation of silicon atoms into the aluminophosphate framework structure in order to modify the acidic properties of SAPO-11 molecular sieve [18-29].Hierarchical SAPO-11 molecular sieves with high activity and selectivity in hydroisomerization of C_{7+} n-paraffins were synthesized [30-40].

It should be noted that one of the main interests in the field of the synthesis of SAPO-n molecular sieves, including SAPO-11, is related to the control of their acidic properties through various mechanisms of introducing silicon atoms [41]. To enhance the process of incorporation of silicon atoms into the SAPO-11 crystal lattice, several approaches have been reported, e.g. use

of different Si sources [18,19], different templates [20-23], crystallization modes [24,25], use of organic solvent [26], crystallization in two-phase systems [27,29] or the DGC method [29].

Zhichao Yang et al. [19] studied the influence of various silicon sources (TEOS, SiO_2 sol, fumed silica) on the incorporation of Si atoms into the SAPO-11. The use of TEOS resulted in the highest Si content in the SAPO-11 material. The authors suggest that due to the monomeric nature of the silica species, they were easily hydrolyzed and incorporated into the SAPO-11 framework structure. Additionally, the TEOS resulted in the synthesis of SAPO-11 with larger silicate islands compared to the crystals synthesized with colloidal and fumed silica. The use of fumed silica was found to produce SAPO-11 with the highest concentration of moderate BAS, through incorporation of silicon by silicate islands of smaller size.

P. Liu et al. [23] studied the influence of the nature of the organic templates (diethylamine, di-n-propylamine, diisopropylamine) and their mixtures (diethylamine + diisopropylamine) on the process of incorporation of silicon atoms into the SAPO-11. The templates, according to the capacity for single incorporation of silicon atoms, were found to be arranged in the following order: mixture (diethylamine + diisopropylamine) → di-n-propylamine → diisopropylamine → diethylamine. While Zheming Wang et al. [26] studied the impact of the nature of silicon source on the acidic properties of the SAPO-11 synthesized in ethylene glycol and glycerin. Crystallization in nonaqueous media proved to offer a higher Si content in the crystallization products due to slow diffusion of the silicon source into growing crystals, ensuring better incorporation. The SAPO-11 samples using TEOS were found to contain more silicon than the samples prepared with colloidal and fumed silica, resulting in the formation of materials with a higher concentration of acid sites. T. Blasco et al. [28] proposed the crystallization in a two-phase system water-hexanol-surfactant (Hexadecylamine) in order to increase the share of single insertion of silicon atoms into the SAPO-11 lattice. This approach resulted in SAPO-11 with a high concentration of silicon atoms with an environment of Si (nAl, 4-nSi), $0<n<4$, while the synthesis in an aqueous medium resulted in the formation of SAPO-11 with larger silicate islands with a predominant environment of Si (4Si). Overly a little attention was paid to the silicon incorporation mechanism, crystals morphology and acidic properties of SAPO-11 crystals. In addition, a limited information on the influence of the nature of silicon source on its dispersion in the crystalline material is paid. In order to create highly efficient SAPO-11 catalyst, it is necessary to control not only the acid sites but also to ensure effective diffusion, which is poorly studied for SAPO-11.

In this work, we report on the use of a silica sol with a particle size of ~ 4 nm as a source of silicon, prepared by a sol-gel method. The use of this silica sol allowed to significantly increase the concentration of acid sites due to the high silicon content and reduced particle size

of the SAPO-11 crystals. The catalytic performance of the SAPO-11 crystals in the dimerization of a-methylstyrene reaction was studied.

2. Experimental

2.1 Synthesis of SAPO-11molecular sieve

SAPO-11 silicoaluminophosphate samples were hydrothermally synthesized from a reaction gel with the following chemical composition: $1.0Al_2O_3 \bullet 1.0P_2O_5 \bullet 0.3SiO_2 \bullet 1.0DPA \bullet 40H_2O$. Orthophosphoric acid (85%, H_3PO_4, Reachem), pseudoboehmite (PB, 77% Al_2O_3, Plural Sasol SB), and di-n-propylamine (99%, DPA, AcrosOrganics) were used as a source of phosphorus, aluminum, and template, respectively. Fumed silica (FS, SIGMA), colloidal silica (Ludox AS-40, SIGMA) and SiO_2 sol (SG) with particles of 200-300 nm, 22 nm and 4 nm were applied as a source of silicon, for the synthesis of SAPO-11, respectively.

Preparation of SAPO-11 with SiO_2 sol (SG): 0.9 g distilled water and 0.2 g of orthophosphoric acid (85%, H_3PO_4, Reachem) were added to 5 g of isopropyl alcohol (99%, AcrosOrganics) as an acid hydrolysis catalyst. 2.7 g of tetraethylorthosilicate (TEOS, 99%, AcrosOrganics) was added to the resulting solution under vigorous stirring. When all the components were mixed, the resulting mixture was kept in a thermostat at 60 °C for 2-3 hours.

The synthesis of SAPO-11 with other silica sources was carried out as follows: 35.6 g of distilled water was added to 10.0 g of orthophosphoric acid. 5.5 g of pseudoboehmite (PB) was subsequently added to the mixture and stirred vigorously for 1 h. Then, 4.4 g of di-n-propylamine was added to the resulting gel. Finally the SiO_2 source was slowly added into the resulting gel. The resulting silicoaluminophosphate gel was vigorously stirred for 1 hour and kept in a thermostat at 90 °C for 24 hours. Preliminary experiments have shown that aging of the gels prevents formation of non-porous tridymite. The gels were then subjected to crystallization at 200 °C for 12 hours in stainless steel autoclaves with a special fluoroplastic coating. After the crystallization was accomplished, the SAPO-11 samples were washed with distilled water to neutral pH, centrifuged, and dried at 100 °C for 48 h. $AlPO_4$-11 was synthesized in the same way as SAPO-11 without introducing the silicon source.

To study the kinetics of SAPO-11 crystallization from mixtures with various silicon sources, the crystallization time was counted from the moment when the autoclaves were subjected to heating.

The silicoaluminophosphate gels were named SAPO(FS), SAPO(SS), SAPO(SG), where FS (fumed silica), SS (colloidal Ludox AS-40), and SG (Sol-Gel SiO_2) correspond to the silicon

sources used. The SAPO-11 samples prepared from the corresponding gels were named as SAPO-11(FS), SAPO-11(SS) and SAPO-11(SG).

2.2 Characterization

The chemical composition of the silicoaluminophosphate gels and crystalline products was characterized by X-ray fluorescence spectroscopy recorded on a Shimadzu EDX 7000P spectrometer.

The particle size distribution of the SiO_2 sol (less than 5 nm in size) was determined by small-angle X-ray scattering (SAXS). Small-angle scattering curves of the samples were obtained using a HECUS bench-scale setup with the X-ray tube equipped with a copper anode of the wavelength of λ (CuKα) = 1.54 Å as the radiation source. Processing of the small-angle scattering curves was performed following a previously reported procedure [42]. The distribution of SiO_2 particles (larger than 5 nm) was assessed by the Photon-Cross-Correlation Spectroscopy-technique (PCCS) with a Nanophox® particle size analyzer.

Powder X-ray diffraction patterns of as-synthesized SAPO-11 samples were recorded on a Bruker D8 Advance diffractometer in CuKα radiation. The patterns were collected over a 2θ range from 5° to 40°. The phase analysis of the obtained X-ray diffraction patterns was performed by the Eva program using the PDF2 database.

The size and morphological features of SAPO-11 crystals were analyzed by field emission scanning electron microscopy (FE-SEM) with a Hitachi Regulus SU8220 scanning electron microscope. The images were taken in the mode of registration of secondary electrons at 5 kV accelerating voltage.

The BET surface area, the volume of micro- and mesopores were measured by the method of low-temperature nitrogen adsorption-desorption with a Nova 1200e sorptometer. The specific surface area was calculated by the multipoint BET method. The micropore volumes in the presence of mesopores were derived from a *t*-Plot approach. The pore size distribution was calculated by the BJH (Barrett-Joyner-Halendy) model from the desorption branch. Prior to the analysis, the samples were calcined at 600 ^{o}C for 6 hours.

The coordination environment of silicon atoms was determined using ^{29}Si MAS NMR spectroscopy. The spectra were collected with a Bruker Avance-400 NMR spectrometer. The resonance frequency for ^{29}Si was 79.49 MHz. The spectra were recorded at 2 μs pulse duration and relaxation delay of 2 s.

The acid properties were analyzed by the NH_3-TPD with a quantachrome Autosorb instrument. The calcined SAPO-11 samples were pretreated at 600 °C in a helium flow for 5 hours, then 10 vol% NH_3 in helium was introduced at 100 °C for 2 hours. The samples were

purged with helium to remove physically adsorbed ammonia. Desorption of NH_3 was controlled in the range from 100 to 600 °C at a heating rate of 10 °C/min. The concentration of weak and moderate acid sites was determined by the amount of desorbed NH_3 (μmol/g) from 100 to 250 °C, from 250 to 400 °C, from 400 to 600 °C, respectively.

The IR spectra using pyridine as a probe molecule were collected with a Bruker Vertex-70V FT-IR spectrometer. Parameters used in measurements were: resolution 4 cm^{-1}, spectral range 400–4000 cm^{-1}. The diameter of the pellet for recording the IR spectra was 10 mm, and the adsorption of pyridine was carried out at 423 K for 30 minutes, followed by removal of physisorbed pyridine by evacuation at 423 K for 30 minutes. The Brønsted acid sites (BAS) were quantified by integrating the peak at 1545 cm^{-1} and Lewis acid sites (LAS) at 1454 cm^{-1}using the molar extinction coefficients of pyridine for each type of sites reported earlier [43].

2.3 Evaluation of catalytic properties of SAPO-11 in the dimerization of α-methylstyrene

Dimerization of α-methylstyrene was carried out in an isothermal batch reactor under stirring at 25 °C in chlorobenzene (99%, Acros Organics) for 2-6 h. The weight concentration of α-methylstyrene in the solution was 20%. The weight concentration of the catalyst based on α-methylstyrene was 10%. The catalyst (80-100 μm fraction of the calcined SAPO-11 sample) was kept in a flow of dried helium at 350 °C for 3 hours before the reaction. Upon the completion of the reaction, the catalyst was removed from the reaction mixture by filtration. The reaction products were characterized by gas-liquid chromatography (GLC) using a HRGS 5300 Mega Series “Carlo Erba” chromatograph with a flame ionization detector (the glass capillary column of 25 length, the SE-30 phase, temperature of analysis of 50–280 °C, programmed heating of 8 °C min^{-1}, detector temperature of 250 °C, evaporator temperature of 300 °C, flow rate of helium carrier gas of 30 mL/min).

2. Results and discussion

In the vast majority of works on the synthesis of SAPO-11, colloidal silica (Ludox SiO_2) or fumed silica with particle size of 10–40 nm or 100–300 nm, respectively, were used as silica source [41]. The rate of depolymerization of the SiO_2 source during the crystallization of SAPO-11 depends on the particle size. Therefore, we assumed that SiO_2 sol with a significantly smaller particle size could significantly change the depolymerization process and increase the efficiency of incorporation of silicon atoms into the alumophosphate precursor mixture and in the ultimate crystalline SAPO framework.

The sol-gel method was used to control the particle size of SiO_2 in a wide range by varying the alkalinity (pH) of the media. [44] In order to prepare homogeneous SiO_2 particles in the sol,

hydrolysis and condensation processes should be carried out in an acidic medium. Figure 1 illustrates particle size distribution of SiO_2 sol prepared by the sol-gel method in an acidic medium and commercial SiO_2 sources (colloidal and fumed silica) based on SASX and PCCS. The particles in the sol-gel SiO_2 sol is about ~ 4 nm, while the colloidal SiO_2 (AS-40) contains particles of ~ 22 nm and the fumed silica of ~ 200 nm.

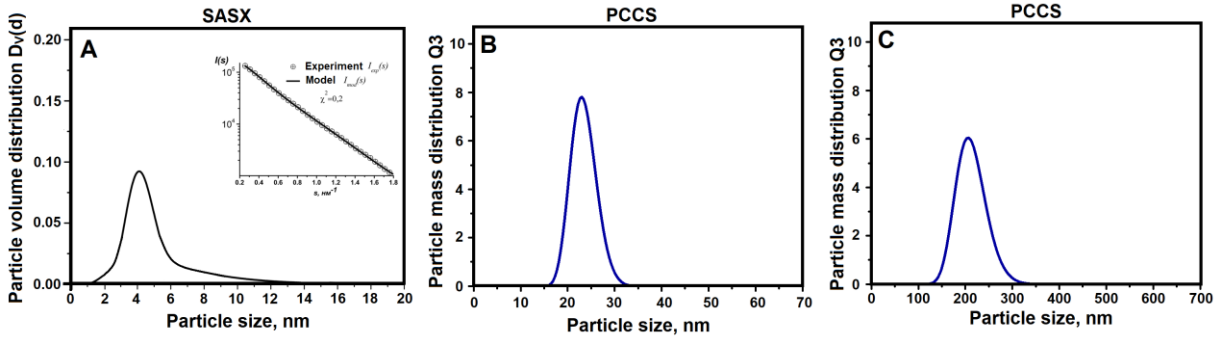

Figure 1. SASX and PCCS particle size distribution of (A) sol-gel SiO_2 sol; (B) colloidal SiO_2 AS-40 sol; and (C) fumed silica.

These three silica sources were used for synthesis of SAPO-11; the X-ray powder diffraction patterns of the samples are shown in Figure 2. For comparison, the AlPO-11 free of silica was synthesized too. All samples exhibit high phase purity and the XRD patterns correspond to the AEL framework topology with a high degree of crystallinity of more than 92% (Table 1). Thus, all the silicon sources applied in the present study resulted in SAPO-11 materials with a high degree of crystallinity. More detailed comparison of the XRD patterns of the SAPO-11 samples reveals differences in the ratio of the intensities of the peaks (020), (200), and (002). Earlier, Li et al [45] attributed this to the different morphology of SAPO-11 crystals.

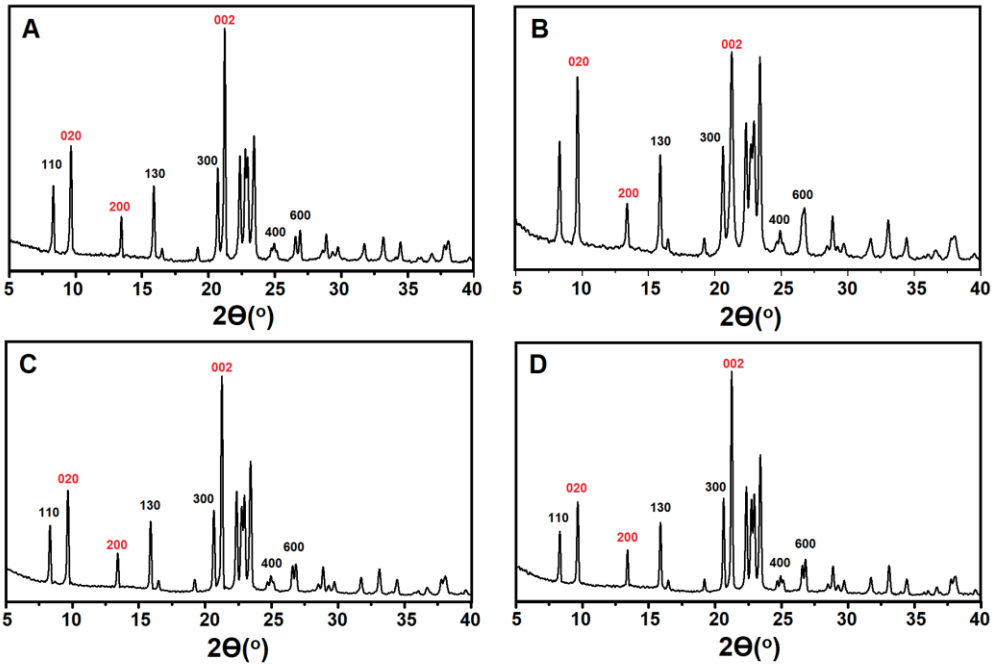

Figure 2. XRD patterns of (A) $AlPO_4$-11; (B) SAPO-11(SG); (C) SAPO-11(SS); and (D) SAPO-11(FS) samples.

Table 1. Effect of SiO_2 sources on the chemical composition and crystallinity of SAPO-11 samples

		Initial gel	Crystalline sample	
Sample	Size SiO_2, nm	Al_2O_3*P_2O_5*SiO_2	Al_2O_3*P_2O_5*SiO_2	*DC
$AlPO_4$-11	-	1.00*0.99	1.00*0.98	95
SAPO-11(SG)	4	1.00*0.98*0.29	1.00*0.92*0.23	92
SAPO-11(SS)	22	1.00*0.98*0.30	1.00*0.93*0.19	94
SAPO-11(FS)	202	1.00*0.97*0.29	1.00*0.96*0.17	94

*DC – degree of crystallinity

As previously reported, the acidic properties of the resulting material depend heavily on the silicon content in the framework of SAPO-n molecular sieves. The elemental compositions of the initial silicoaluminophosphate gels and crystalline SAPO-11 prepared by different SiO_2 sources are summarized in Table 1.The silicon content in the initial gels is higher than in the SAPO-11 samples. The results are attributable to the fact that silicon is characterized by weak capacity for incorporation into the aluminophosphate lattice and part of it remains in the mother liquor after the crystallization. It should be noticed that silicon content in the SAPO-11increases while reducing the size of SiO_2 particles of the initial precursor. This result can be due to the increased rate of depolymerization of SiO_2 particles and more efficient incorporation of silicon

into the AEL aluminophosphate lattice. In addition, the SiO_2 particle size in the precursosrs affects the morphology of the SAPO-11 crystals. The SEM images for SAPO-11 samples obtained by different silica sources are depicted in Figure 3. A decrease in the size of the SiO_2 particles was found to cause a significant change in the morphology and a decrease in the size of the crystals. Indeed, the SAPO-11 sample prepared using the fumed silica with the largest SiO_2 particles is characterized by crystals of 1–2 μm and an elongated prism morphology. The use of colloidal silica with a particle size of 22 nm resulted in SAPO-11 crystals with a size of 0.5-1 μm and similar morphology. The use of SiO_2 sol with a particle size of ~ 4 nm resulted in intergrown SAPO-11 crystals of size of 100-300 nm in the form of cubes and prisms. The results show that the silica precursors effect significantly not only the size but also the morphology of the SAPO-11 crystals.

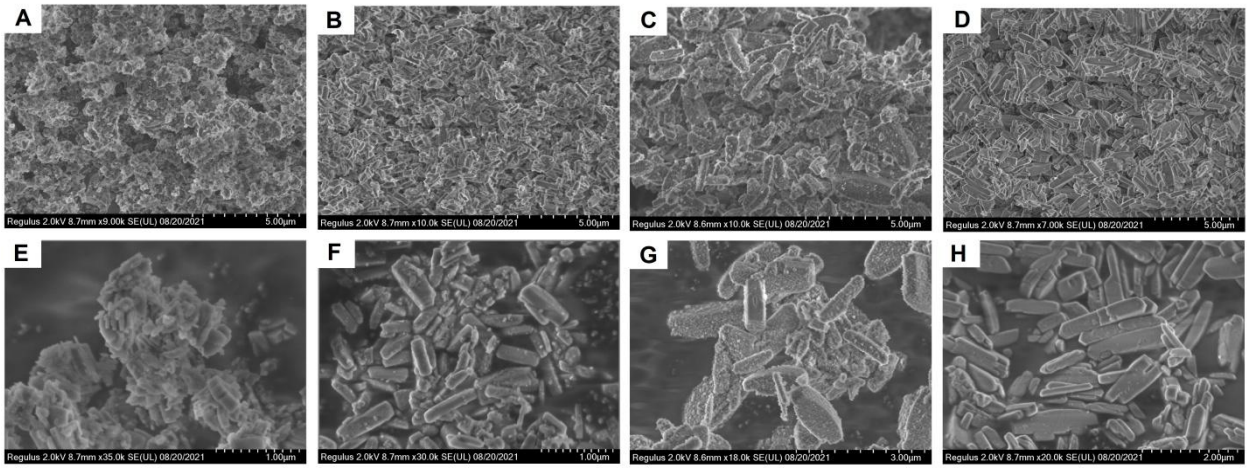

Figure 3. SEM images of (A) SAPO-11(SG) sample (magnification x9.00); (B) SAPO-11(SS) sample (magnification x10.00); (C) SAPO-11(FS) sample (magnification x10.00); (D) $AlPO_4$-11 sample (magnification x7.00); (E) SAPO-11(SG) sample (magnification x35.00); (F) SAPO-11(SS) sample (magnification x30.00); (G) SAPO-11(FS) sample (magnification x18.00); (H) $AlPO_4$-11 sample (magnification x20.00).

Nitrogen adsorption-desorption isotherms and pore size distribution analyses of the SAPO-11 samples are presented in Figure 4; the results deduced from the measurements are summarized in Table 2. Isotherms close to type I are observed for SAPO-11(FS) and $AlPO_4$-11 samples with a weak hysteresis loop at high pressure. This type of isotherm is typical for microporous materials. An isotherm close to type IV is measured for SAPO-11(SG) and SAPO-11(SS) samples, characteristic of micro-mesoporous materials. All the samples exhibit a wide distribution of mesopores from 2 to 30 nm, while the SAPO-11(SG) sample has a maximum in the region of 20 nm. The decrease in the size of SiO_2 particles in the precursors increases the specific surface area and mesopore volumes of the ultimate crystalline SAPO-11 samples. These

results are attributed to a decrease in the size of the SAPO-11 crystals. The SAPO-11 (SG) sample exhibits the highest specific surface area and mesopore volume (Table 2).

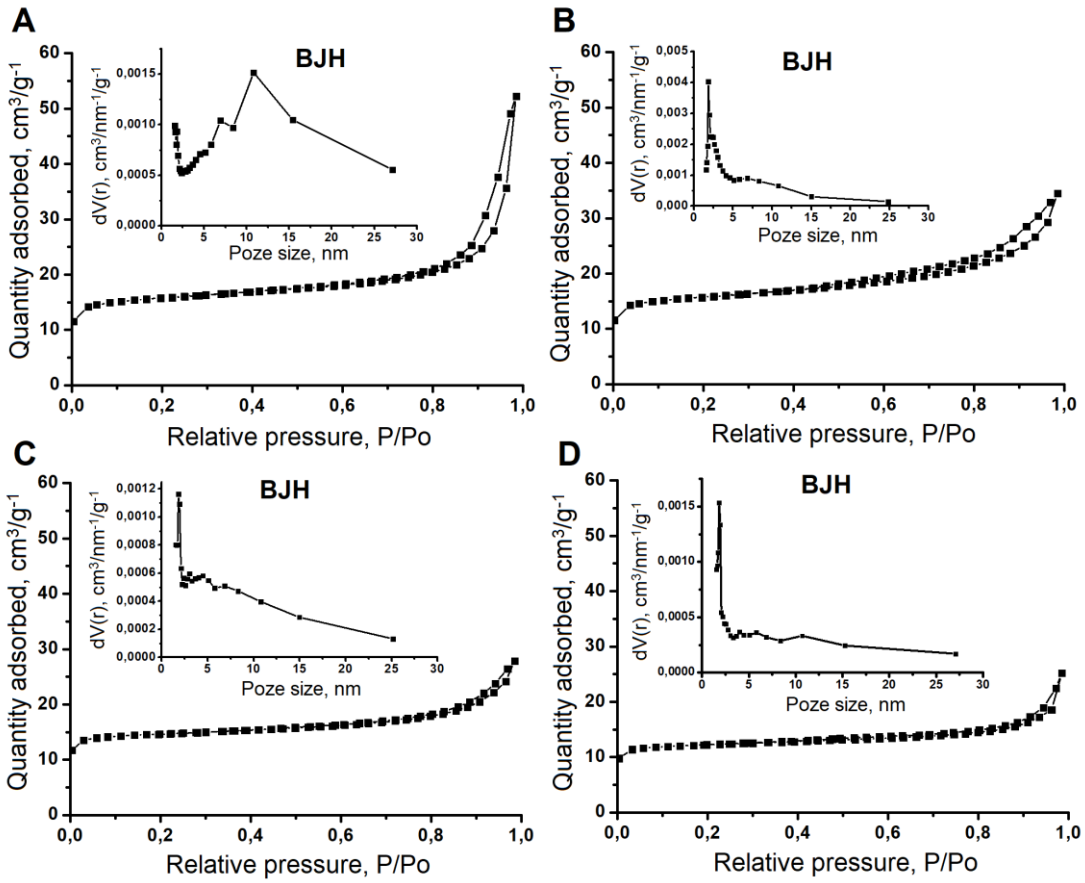

Figure 4. N_2 adsorption-desorption isotherms and pore size distribution of (A) SAPO-11(SG) sample; (B) SAPO-11(SS) sample; (C) SAPO-11(FS) sample; (D) $AlPO_4$-11 sample.

Table 2. Characteristics deduced from the N_2 sorption measurements of SAPO-11 and $AlPO_4$-11 samples.

Sample	S_{BET}, m^2/g	S_{EX}, m^2/g	V_{micro}, cm^3/g	V_{meso}, cm^3/g
SAPO-11(SG)	250	120	0.067	0.27
SAPO-11(SS)	235	105	0.066	0.15
SAPO-11(FS)	204	70	0.070	0.09
$AlPO_4$-11	190	65	0.065	0.09

Symbols:

(S_{BET}) BET specific surface area

(S_{EX}) external specific surface

(V_{micro}) specific micropore volume

(V_{Σ}) total pore volume

The silicon precursor sources with various size of the SiO_2 particles may control the size, morphology and porosity of the crystalline SAPO materials. This can be attributed to the fact that the size of SiO_2 particles at the initial stages of crystallization has a significant impact on the nucleation and subsequent growth rates. We assumed that highly dispersed SiO_2 during the nucleation stage may lead to higher concentration of silica monomers and oligomers thus leading to an increased silicon content into the SAPO-11 framework and further slowdown the crystal growth. To confirm this hypothesis, we studied the crystallization kinetics of SAPO-11 with samples with various SiO_2 sources (Figure 5). It can be seen that the duration of the induction period for the SAPO-11 (SG) sample is twice as long as for the SAPO-11 (SS) and SAPO- (FS) samples, which indicates a slowdown in the growth rate of SAPO-11 crystals with a decrease in the SiO_2 particle size. The shortest induction period of SAPO-11 is measured for the sample synthesized with fumed silica (300-400 nm).

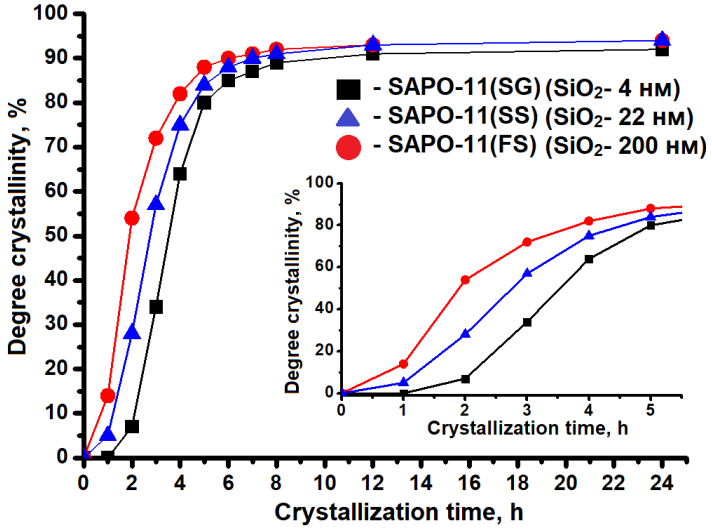

Figure 5. Degree of crystallinity as a function of time for SAPO-11(SG), SAPO-11(SS), SAPO-11(FS) samples. *Inset:* degree of crystallinity of samples up to 5 h representing the nucleation and initial stage of crystallization of the samples.

The reported data show that the strength and concentration of Brønsted acid sites in SAPO molecular sieves depend on the mechanism of silicon incorporation into the aluminophosphate framework ~~(SM)~~ [46].

~~The conventional strategies applied for introduction of silicon in $SAPO_n$ are SM2 and SM+SM3 types. As applied to the SM2 mechanism, a single insertion of silicon atoms Si (0Si,4Al) occurs to form the highest amount of Brønsted acid sites. As for the SM2+SM3 types, the so-called silicate islands of various sizes are formed, with the environment of Si (4Si,0Al) typical for silicon in the centre, and Si(4−nSi, nAl)(n≥1) at the boundaries. The formation of Brønsted acid sites in the case of the SM2+SM3 mechanism occurs only at the boundary of~~

~~silicate islands, while the formed BAS are supposed to be stronger than those formed by the SM2 type [8].~~

The ^{29}Si MAS NMR spectra of the SAPO-11 samples synthesized with various silicon sources are depicted in Figure 6; the results from the deconvolution of the spectra are shown in Table 3. A wide signals from -86 to -112 ppm are observed in all samples. The obtained spectra were deconvoluted into 6 signals based on Gaussian components . The peaks at -91, -97, -102, -107 and -112 ppm are assigned to silicon atoms with the environment of Si (0Si, 4Al), Si (1Si, 3Al), Si (2Si, 2Al), Si (3Si, 1Al) and Si (4Si, 0Al), respectively [23,37]. [47]. The results point out that a reduction of the particle size of the silicon precursor source leaded to an increase of the size of the silicate islands. SAPO-11(FS) sample exhibits the highest signal intensity at -112 ppm, indicating the presence of larger silicate islands. For the SAPO-11(SG) sample, the highest total signal intensity is observed from -97 to -107 ppm, which indicates the predominance of smaller silicate islands than in the SAPO-11(SS) and SAPO-11(FS) samples. These results are attributed to the fact that smaller SiO_2 particles depolymerize faster, and silicon is more efficiently incorporated into the aluminophosphate framework forming smaller silicate islands. It is important to note that for all SAPO-11 samples obtained using various silicon sources, there is a close proportion of silicon atoms introduced by the SM2 mechanism (signal at -91 ppm), about ~ 28%. Apparently, this fraction is associated with the limited capabilities of silicon atoms to be incorporated by the SM2 mechanism into the SAPO-11 lattice.

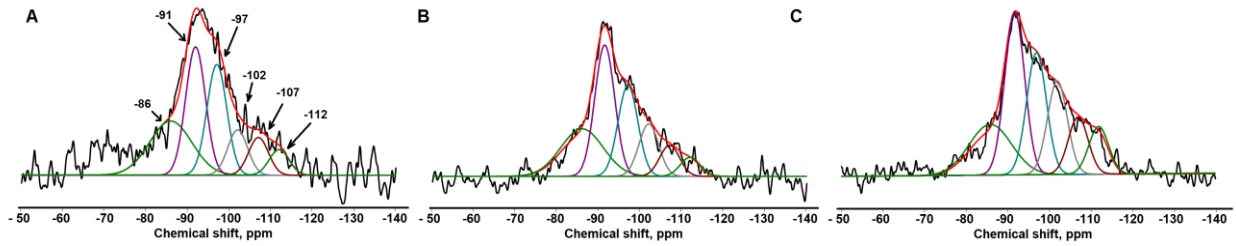

Figure 6. ^{29}Si MAS NMR spectra of (A) SAPO-11(SG); (B) SAPO-11(SS); and (C) SAPO-11(FS) samples.

Table 3. Results from the deconvolution of ^{29}Si MAS NMR spectra of SAPO-11 samples.

	Deconvolution (%)					
Sample	Si(OH) or $Si(OH)_2$, -86 ppm	Si (0Si, 4Al), - 91 ppm	Si (1Si, 3Al), -97 ppm	Si (2Si,2Al), -102 ppm	Si (3Si, 1Al), -107 ppm	Si (4Si, 0Al), -112 ppm
SAPO-11(SG)	25	28	24	10	8	5
SAPO-11(SS)	25	30	19	12	7	6
SAPO-11(FS)	18	28	20	16	10	8

The SAPO-11 silicoaluminophosphate molecular sieves with one-dimensional channel structure possess *moderate* acid sites. The TPD-HN_3 and IR spectra recorded on the SAPO-11 samples are presented in Figure 7 and Figure 8, respectively The concentrations of Brønsted (BAS) and Lewis (LAS) acid sites and the data derived from the TPD-NH_3 measurements are summarized in Table 4. The absorption bands corresponding to pyridine adsorbed on Brønsted acid sites (BAS) and Lewis acid sites (LAS) at 1545 and 1454 cm^{-1}, respectively are observed in all spectra [48]. Both sites contribute to the appearance of the absorption band at 1490 cm^{-1}. An increase in the concentration of both acid sites with a decrease in the size of SiO_2 precursor used for the synthesis is observed. The use of SiO_2 particles of ~ 4 nm practically double the concentration of both types of acid sites, and triples the concentration of strong acid sites(according to the TPD- NH_3. The results is explained with the more efficient incorporation of Si into the aluminophosphate framework. The TPD- NH_3 and IR results are in good agreement with the ^{29}Si MAS NMR data indicating that the smallest silica precursors particles contribute to the reduction of the size of silicate islands and increase the concentration of acid sites in the SAPO-11 materials.

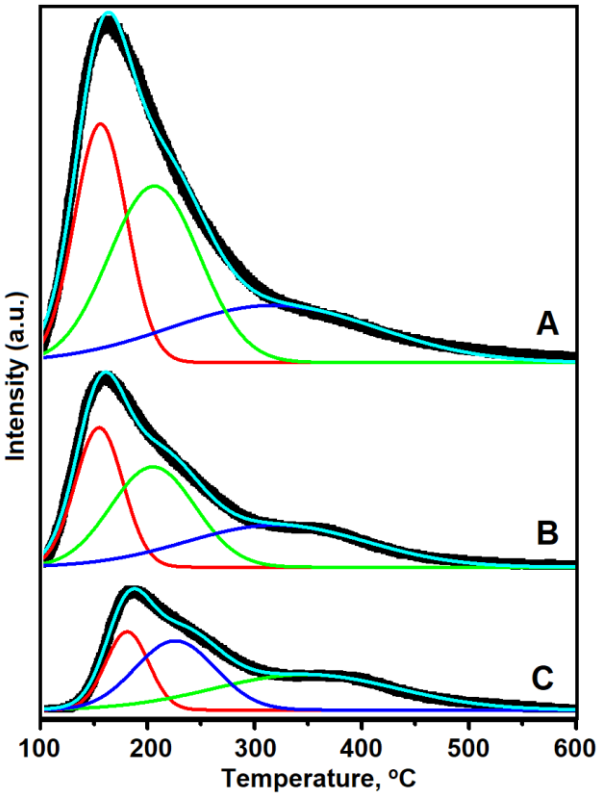

Figure 7. TPD-NH_3 spectra of (A) SAPO-11 (SG); (B) SAPO-11 (SS); and (C) SAPO-11 (FS) samples.

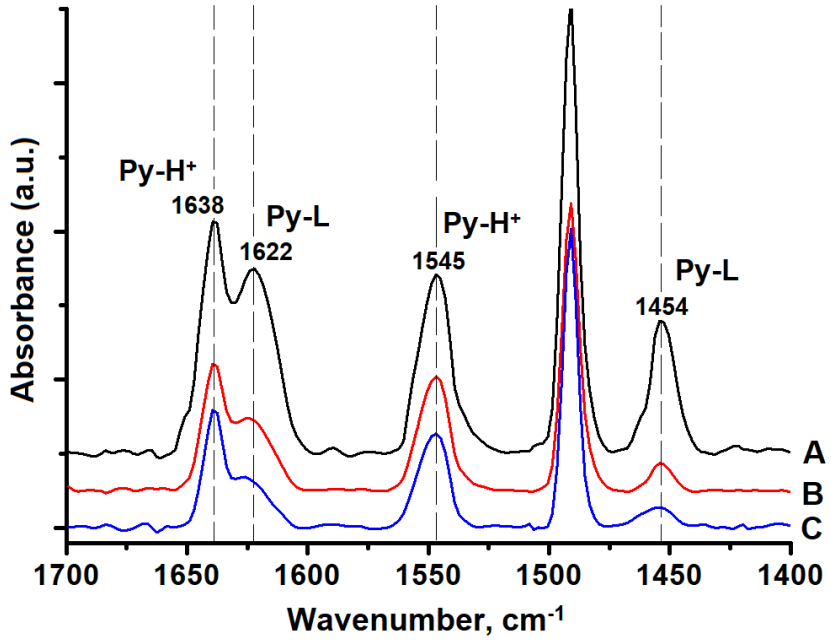

Figure 8. IR spectra of adsorbed pyridine on calcined (A) SAPO-11 (SG); (B) SAPO-11 (SS); and (C) SAPO-11 (FS) samples.

Table 4. Acidic properties of SAPO-11 samples synthesized with different silica sources

	*Acidity (μmol/g)			**Acidity (μmol/g)		
sample	BAS	LAS	B/L	Weak	Medium	Strong
SAPO-11(SG)	121	51	2.3	288	368	273
SAPO-11(SS)	98	13	7.5	128	163	146
SAPO-11(FS)	74	10	7.4	64	125	106

B/L – BAS/ LAS

* - concentration of acid sites calculated based on IR-Py

** - concentration of acid sites calculated based on NH_3 -TPD

Most of the considered application of SAPO-11 molecular sieve in catalysis is associated with the hydroisomerization of C_{7+} n-paraffins. Earlier [49], we reported on the SAPO-11 as highly selective catalyst for production of linear dimers of α-methylstyren representing valuable petrochemical products applied as regulators of the growth of polymer chains, plasticizers of polymers and rubbers, dielectric fluids, synthetic oils, etc. [50]. As reported previously [50], dimerization of α-methylstyrene in the presence of zeolite catalysts proceeds to form linear (I, II) and cyclic (III) dimers (Scheme 1).

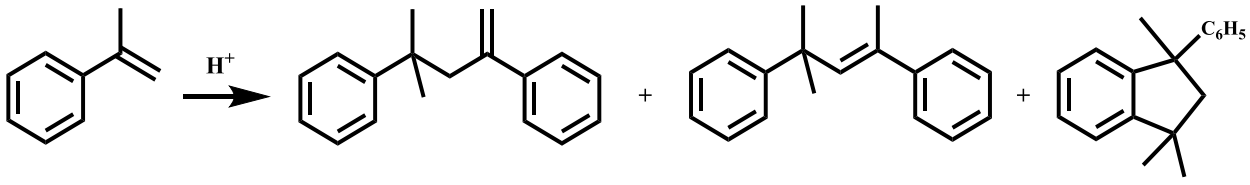

I II III

The results of dimerization of α-methylstyrene using the SAPO-11 samples synthesized using various SiO_2 sources are summarized in Table 5. As expected, the $AlPO_4$-11 sample does not show catalytic activity in this reaction due to the very low concentration of acid sites. The main reaction products for all SAPO-11 samples are a-methylstyrene dimers: trans-4-methyl-2,4-diphenylpent-2-ene (I), 4-methyl-2,4-diphenylpent-1-ene (II) , and 1,1,3-trimethyl-3-phenylindane (III). The SAPO-11(SG) sample exhibited the maximum activity in the reaction, assessed by the conversion of a-methylstyrene. Here, the monomer conversion reaches 92.4% after 6 h. While the SAPO-11(SS) sample was less active, and the SAPO-11(FS) sample showed the lowest activity. The dimer composition using the SAPO-11(SG) and SAPO-11(SS) samples is similar: the main compounds are linear dimers (I), and the selectivity of 90.7% and 92.3% measured after 6 h, respectively was reached. The increase in the amount of cyclic dimer (III) under increasing the reaction time is attributed to the fact that, intramolecular alkylation of linear dimers occurs in the presence of acid catalysts and they are irreversibly converted into cyclic dimer (III). The dimers formed in the SAPO-11(FS) sample contain a significant amount of cyclic dimer up to 39.7% (Table 5).

The comparison of the catalytic and physicochemical properties of the samples under study reveals symbatic change of the activity of the catalysts with the concentration and strength of acid sites. Consequently, the concentration and strength of acid sites decreases in the following order: SAPO-11(SG)> SAPO-11(SS)>SAPO-11(FS), the activity of the samples in the reaction changes in the same sequence. The different selectivity in the formation of linear and cyclic dimers is due tomnot only differences in acidic properties but also in the porosity of the samples. The highest selectivity for linear dimer (I), as well as linear dimers I and II is measured for micro-mesoporous SAPO-11(SG) and SAPO-11(SS) samples. Apparently, the presence of mesopores makes it easier for α-methylstyrene molecules to reach the acid sites located in micropores, where linear dimers are formed, ensuring their reverse diffusion into the reaction volume as well. Few surface acid sites are available for the reacting molecules in the microporous SAPO-11 (FS) sample, while the acid sites located inside the channels are inaccessible. This explains the low activity of the SAPO-11 (FS) sample. The surface acid sites offer more favorable conditions for the formation of bulky molecules of cyclic dimer III than the narrow microporous channels of the SAPO-11 catalyst.

Table 5. Dimerization of a-methylstyrene using SAPO-11 catalysts synthesized with different silica precursors.

Sample	t, h	$X_{a\text{-}MS}$, %	S_I, %	S_{II}, %	S_{III}, %
$AlPO_4$-11	2	-	-	-	
	6	-	-	-	-
SAPO-11(SG)	2	47.8	92.4	4.0	3.6
	6	92.4	90.7	4.5	4.8
SAPO-11(SS)	2	12.6	97.1	2.6	0.3
	6	21.4	92.3	2.5	5.2
SAPO-11(FS)	2	4.5	53.4	8.5	38.1
	6	8.6	51.2	9.1	39.7

Symbols:

($X_{a\text{-}MS}$) a-methylstyrene conversion

(S_I) Selectivity for linear dimer I

(S_{II}) Selectivity for linear dimer II

(S_{III}) Selectivity for cyclic dimer III

Conclusion

In summary, the synthesis of SAPO-11 molecular sieve using silica precursors with different particle sizes (fumed silica, colloidal silica and sol-gel SiO_2 sol) was carried out. The results show that all the three silica sources were appropriate for the synthesis of SAPO-11 material with high phase purity and high degree of crystallinity. An increase in the silicon content in the SAPO-11 sample synthesized with the sol-gel SiO_2 sol with the smallest particle size was observed. This SiO_2 sol with a size of particles of 4 nm proved to be the most appropriate for the depolymerization of the silica source and lead to more efficient incorporation of Si into the SAPO-11 framework. As a result, the size of silicate islands in the SAPO-11 material decreases, followed by consequent increasing the concentration of acid sites.

The effect of the particle size of the SiO_2 sol on the crystallization kinetics of SAPO-11 has been observed. With decrease of the size of SiO_2 particles, a decrease in the rate of crystallization of SAPO-11 and an increase in the induction period of formation of nuclei are observed.

The size of SiO_2 particles was found to have a significant impact on the size and morphology of the final SAPO-11 crystals, as well as on their mesoporosity. A decrease in the size of SiO_2 particles of silicon sources is followed by a decrease in the size of crystals and a change in their morphology from prisms to cubic. The use of silica sol (particle size of ~ 4 nm)

resulted in intergrown SAPO-11 crystals of 100-300 nm in size with a hierarchical pore structure (S_{BET} – 250 m^2/g, V_{meso} – 0.27 cm^3/g).

The prospects of using SAPO-11 with an increased concentration of acid sites and a hierarchical pore structure as a catalyst for the highly selective synthesis of linear a-methylstyrene dimer, 4-methyl-2,4-diphenylpent-1-ene, was disclosed. SAPO-11 samples with a hierarchical pore structure (SAPO-11(SG) and SAPO-11(SS)) provide the highest selectivity for the formation of linear dimer (I) compared to the microporous SAPO-11(FS) sample. The maximum yield of linear dimer I (83.8%) was achieved using the SAPO-11(SG) catalyst with the maximum concentration of acid sites and hierarchical pore structure, ensuring efficient diffusion of the monomer to active sites, reverse diffusion of reaction products, and formation of linear dimers.

Acknowledgments

The study was supported by a grant from the Russian Science Foundation No. 21-13-00169, https://rscf.ru/project/21-13-00169/

References

[1] Pat. US 4440871 (1984).

[2] P. Tian, Y. Wei, M. Ye, Z. Liu, ACS Catal. 5 (2015) 1922-1938. https://doi.org/10.1021/acscatal.5b00007

[3] S.J. Miller, Micropor. Mater. 2 (1994) 439-449. https://doi.org/10.1016/0927-6513(94)00016-6

[4] S.J. Miller, Stud. Surf. Sci. Catal. 84 (1994) 2319-2326. https://doi.org/10.1016/S0167-2991(08)63796-9

[5] C. Baerlocher, W.M. Meier, D.H. Olson, Atlas of zeolite framework types, 6th ed., Elsevier, Amsterdam, 2007.

[6] E.M. Flanigen, B.M. Lok, R.L. Patton, S.T. Wilson, Pure Appl. Chem. 58 (1986) 1351-1358. https://doi.org/10.1016/S0167-2991(09)60862-4

[7] G. Sastre, D.W. Lewis, C.R.A. Catlow, J. Phys. Chem. 100 (1996) 6722-6730. https://doi.org/10.1021/jp953362f

[8] D. Barthomeuf, Zeolites 14 (1994) 394-401. https://doi.org/10.1016/0144-2449(94)90164-3

[9] R. Yadav, A. Sakthivel, Appl. Catal. A: Gen. 481 (2014) 143-160. https://doi.org/10.1016/j.apcata.2014.05.010

[10] H. Deldari, Appl. Catal. A: Gen. 293 (2005) 1-10. https://doi.org/10.1016/j.apcata.2005.07.008

[11] W. Wang, Ch.-J. Liu. W. Wu, Catal. Sci. Technol. 9 (2019) 4162-4187. https://doi.org/10.1039/C9CY00499H

[12] P. Meriaudeau, A. Vu Tuan, N. Le Hung, G. Szabo, Catal. Lett. 47 (1997) 71-72. https://doi.org/10.1023/A:1019059727656

[13] P.S. Singh, R. Bandyopadhyay, S.G. Hegde, B.S. Rao, Appl. Catal. A: Gen. 136 (1996) 249-263. https://doi.org/10.1016/0926-860X(95)00303-7

[14] M.R. Agliullin, A.V. Faizullin, A.N. Khazipova, B.I. Kutepov, Kinet Catal 61 (2020) 654-662. https://doi.org/10.1134/S0023158420040011

[15] Z. Zhu, Q. Chen, Z. Xie, W. Yang, C. Li, Micropor. Mesopor. Mater. 88 (2006) 16-21. https://doi.org/10.1016/j.micromeso.2005.08.021

[16] X. Wang, F. Guo, X. Wei, Z. Liu, W. Zhang, S. Guo, L. Zhao, Korean J. Chem. Eng. 33 (2016) 2034-2041. https://doi.org/10.1007/s11814-016-0065-y

[17] M.R. Agliullin, B.I. Kutepov, V.A. Ostroumova, A.L. Maximov, Pet. Chem. 61 (2021) 852-870. https://doi.org/10.1134/S096554412108003X

[18] R. Bértolo, Appl. Catal. A: Gen. 542 (2017) 28-37. https://doi.org/10.1016/j.apcata.2017.05.010

[19] Zhichao Yang, Jilong Li, Yunqi Liu, Chenguang Liu. J. Energy Chem. 26 (2017) 688-694 https://doi.org/10.1016/j.jechem.2017.02.002

[20] P. Liu, Catal. Commun. 9 (2008) 1804-1809. https://doi.org/10.1016/j.catcom.2008.01.030

[21] X. Wang, J. Braz. Chem. Soc. 24 (2013) 1180-1187. https://doi.org/10.5935/0103-5053.20130152

[22] A. Fernandes, F. Ribeiro, J. Lourenço, Z. Gabelica, Stud. Surf. Sci. Catal. 174 (2008) 281-284. https://doi.org/10.1016/S0167-2991(08)80197-8

[23] P. Liu, J. Ren, Y. Sun, Micropor. Mesopor. Mater. 114 (2008) 365-372. https://doi.org/10.1016/j.micromeso.2008.01.022

[24] P. Liu, Chin. J. Catal. 29 (2008) 379-384. https://doi.org/10.1016/S1872-2067(08)60034-0

[25] Y. Lyu, Y. Liu, X. He, L. Xu, X. Liu, Z. Yan, Appl. Surf. Sci. 453 (2018) 350-357. https://doi.org/10.1016/j.apsusc.2018.05.106

[26] Z. Wang, Z. Tian, F. Teng, G. Wen, Y. Xu, Z. Xu, L. Lin, Catal. Lett. 103 (2005) 109-116. https://doi.org/10.1007/s10562-005-6510-x

[27] L. Guo, Y. Fan, X. Bao, G. Shi, H. Liu, J. Catal. 301 (2013) 162-173. https://doi.org/10.1016/j.jcat.2013.02.001

[28] T. Blasco, A. Chica, A. Corma, W.J. Murphy, J. Agúndez-Rodríguez, J. Pérez-Pariente, J. Catal. 242 (2006) 153-161. https://doi.org/10.1016/j.jcat.2006.05.027

[29] B. Chen, Y. Huang, Micropor. Mesopor. Mater. 123 (2009) 71-77. https://doi.org/10.1016/j.micromeso.2009.03.025

[30] F. Zhang, Chem. Commun. 53 (2017) 4942-4945. https://doi.org/10.1039/C7CC01519D

[31] Zh. Chen, W. Song, Sh. Zhu, W. Lai, X. Yi, W. Fang, RSC Adv. 7 (2017) 4656-4666. https://doi.org/10.1039/C6RA26522G

[32] Y. Seo, S. Lee, Ch. Jo, R. Ryoo, J. Am. Chem. Soc. 135 (2013) 8806-8809. https://doi.org/10.1021/ja403580j

[33] G. Majano, K. Raltchev, A. Vicente, S. Mintova, Nanoscale 7 (2015) 5787-5793. https://doi.org/10.1039/C4NR07272C

[34] Ping Zhang, Haiyan Liu, Yuanyuan Yue, Haibo Zhu, Xiaojun Bao. Fuel Processing Technology. 179 (2018) 72–85 https://doi.org/10.1016/j.fuproc.2018.06.012

[35] X. Zhao, W. Liu, J. Wang, W. Yang, X. Zhu, K. Zhu, Appl. Catal. A: Gen. 602 (2020) 117738. https://doi.org/10.1016/j.apcata.2020.117738

[36] Z. Chen, Catal. Commun. 103 (2018) 1-4. https://doi.org/10.1016/j.catcom.2017.09.002

[37] D. Jin, ACS Catal. 7 (2017) 5887-5902. https://doi.org/10.1021/acscatal.7b01646

[38] L. Guo, J. Catal. 294 (2012) 161-170. https://doi.org/10.1016/j.jcat.2012.07.016

[39] L. Yang, H. Li, Jun ying Fu, M. Li, Ch. Miao, Zh. Wang, P. Lv, Zh. Yuan, RSC Adv. 9 (2019) 34457-34464. https://doi.org/10.1039/C9RA06117G

[40] P. Zhang, Fuel Process. Technol. 179 (2018) 72-85. https://doi.org/10.1016/j.fuproc.2018.06.012

[41] M.R. Agliullin, B.I. Kutepov, V.A. Ostroumova, A.L. Maximov, Pet. Chem. 61 (2021) 836-851. https://doi.org/10.1134/S0965544121080028

[42] M.R. Agliullin, I.G. Danilova, A.V. Faizullina, S.V. Amarantov, S.V. Bubennov, T.R Prosochkina, N.G. Grigor'eva, E.A. Paukshtis, B.I. Kutepov, Micropor. Mesopor. Mater. 230 (2016) 118-127. https://doi.org/10.1016/j.micromeso.2016.05.007

[43] M. Tamura, K.-i. Shimizu, A. Satsuma, Appl. Catal. A: Gen. 433 (2012) 135-145. https://doi.org/10.1016/j.apcata.2012.05.008

[44] C.J. Brinker, G.W. Scherer, Sol-gel Science, the Physics and Chemistry of Sol-gel Processing Academic Press, Boston, 1990.

[45] L. Li, K. Shen, X. Huang, Y. Lin, Y. Liu, Micropor. Mesopor. Mater. 313 (2021) 110827. https://doi.org/10.1016/j.micromeso.2020.110827

[46] M.E. Potter, ACS Catal. 10 (2020) 9758−9789. https://doi.org/10.1021/acscatal.0c02278

[47] L. Zhang, Y.N. Huang, J. Mater. Chem. A 3 (2015) 4522−4529. https://doi.org/10.1039/C4TA06775D

[48] A. Palčića, V. Valtchev, Appl. Catal. A: Gen. 606 (2020) 117795. https://doi.org/10.1016/j.apcata.2020.117795
[49] M.R. Agliullin, Z.R. Khairullina, R.Z. Kuvatova, B.I. Kutepov, Catal. Ind. 12 (2020) 89–94. https://doi.org/10.1134/S2070050420020026
[50] N.G. Grigor'eva, E.A. Paukshtis, B.I. Kutepov, R.R. Galyautdinova, U.M. Dzhemilev, Pet. Chem. 45 (2005) 419-425